Available online at www.sciencedirect.com
SCIENCE DIRECT®
Catalysis Today 93–95 (2004) 377–381
CATALYSIS TODAY
www.elsevier.com/locate/cattod

Characterization and activity of stannum modified Hβ catalysts for transesterification of dimethyl oxalate with phenol

Shengping Wang, Xinbin Ma*, Jinlong Gong, Ning Gao, Hongli Guo, Xia Yang, Genhui Xu

Key Laboratory for Green Chemical Technology, School of Chemical Engineering and Technology, Tianjin University, Tianjin 300072, China

Available online 3 July 2004

Abstract

The transesterification of dimethyl oxalate (DMO) with phenol over stannum modified Hβ was conducted to prepare diphenyl oxalate (DPO) used to produce diphenyl carbonate (DPC). The component, structure and phase of Hβ catalysts with various Sn loadings were investigated. The relationship between the catalytic properties and the amount of Sn loadings was discussed. The catalyst of Hβ with 2 wt.% Sn loading based on metal performed best, giving 75.3% conversion of DMO and 24.0% selectivity to DPO. At Sn loadings below 2 wt.%, Sn was highly dispersed as monolayer, but at higher loadings it was crystallized into bulk tin dioxide, and the catalytic activity decreased. The curve of XPS peak intensity ratio of Sn 3d/Si 2p versus Sn loadings estimated the dispersed capacity of Sn on Hβ to be 2.1% Sn loading, which was in good agreement with the value obtained from XRD analysis. NH_3-TPD results showed that the amount of Sn loading had effect only on the strength of the weak surface acid sites on Hβ. And the decrease of selectivity to anisole was not due to the change of the weak acid sites. Maybe, SnO_2 accelerated to the formation of MPO and DPO. FTIR analysis of adsorbed pyridine showed that many Lewis acid sites and few Brönsted acid sites were present on Hβ catalysts with or without Sn modified. The acid sites together with SnO_2 active centers catalyzed the transesterification of DMO with phenol. Especially, SnO_2 active centers were in favor of the disproportionation of MPO into DPO.

Keywords: Diphenyl carbonate; Diphenyl oxalate; Methyl phenyl oxalate; Dimethyl oxalate; Transesterification; Stannum modified Hβ

1. Introduction

Aromatic carbonates have come to occupy an important position as useful organic chemicals for a variety of industrial and synthetic applications. They are used as solvents and as reagents in the transesterification reactions with glycols and bisphenol for the production of polycarbonates (PCs), as chemical intermediates and potential gasoline additives [1].

The industrial methods, which are most commonly employed for the synthesis of aryl carbonates, are based on the reaction between an aromatic alkanol with phosgene in the presence of bases.

Because the current trend in the chemical industry is to reduce the risks connected with the use of highly toxic substances such as phosgene [2], alternative approaches to diphenyl carbonate (DPC) production appear to be both the ester exchange reaction of phenol with dimethyl carbonate or dimethyl oxalate (DMO) and the oxidative carbonylation of the phenol [1–7].

Among them, the transesterification of DMO with phenol via a three-step reaction has been deemed as the most promising and possible routes for DPC synthesis [8,9] from the raw materials such as carbon monoxide, phenol and oxygen. In the first step, dimethyl oxalate is produced by carbonylation of methanol [10]; and then, diphenyl oxalate (DPO) is obtained from the transesterification of DMO with phenol; and in the last, the decarbonylation of DPO is carried out to produce DPC and by-product carbon monoxide [11]. In the second step, the synthesis of diphenyl oxalate (DPO) follows the two-step reaction module consisting of the transesterification of DMO with phenol into methyl phenyl oxalate (MPO) and the further transesterification or the disproportionation of MPO into DPO [8,9].

$$(COOCH_3)_2 + C_6H_5OH \rightarrow C_6H_5OOCCOOCH_3 + CH_3OH \quad (1)$$

$$C_6H_5OOCCOOCH_3 + C_6H_5OH \rightarrow (COOC_6H_5)_2 + CH_3OH \quad (2)$$

* Corresponding author. Tel.: +86 22 27406498; fax: +86 22 27890905.
E-mail address: xbma@tju.edu.cn (X. Ma).

0920-5861/$ – see front matter © 2004 Elsevier B.V. All rights reserved.
doi:10.1016/j.cattod.2004.06.031

$$2C_6H_5OOCCOOCH_3 \rightarrow (COOC_6H_5)_2 + (COOCH_3)_2 \quad (3)$$

The thermodynamic equilibrium constants of Reactions (1), (2) and (3) at 453 K are only 0.23, 4.77×10^{-8} and 2.09×10^{-7}, respectively, from the thermodynamic calculation made with the group contribution on the liquid components. This indicates that the transesterification between DMO and phenol, especially a further transesterification of MPO with phenol and the disproportionation of MPO are not favorable in the thermodynamics. Thus, the equilibrium conversion of DMO is only 32.4% based on the Reaction (1).

Keigo et al. [8,9,11] reported the transesterification of DMO with phenol was carried out in the liquid phase using traditional transesterification catalysts such as Lewis acids and soluble organic Pb, Sn, or Ti compounds. In these homogeneous systems, the separation and recovery of the catalysts remain a critical item when these catalyst systems are applied to the industrial process. So, the development of active solid catalysts is highly desirable in view of regeneration and separation. Unfortunately, there are few reports on the development of active heterogeneous catalysts for the reaction up to present time. The goal of our work, therefore, is to develop a heterogeneous catalytic system that combines good catalytic performance with satisfactory recovery of the catalysts used.

More recently, we found that Hβ can catalyze the transesterification of phenol with DMO to MPO and DPO [12]. The results indicated that the selectivity to DPO was not satisfactory. Moreover, there were quite few further studies on the reaction and the characterization of this new catalytic system. Owing to organic Sn compounds were widely used as disproportionation catalysts [13–15], thus, in this paper, the transesterification of DMO with phenol as well as the characteristic aspects of stannum modified Hβ catalyst was investigated to find immanent correlation between catalytic performance and catalyst structure.

2. Experimental

2.1. Catalysts preparation

Hβ seive was dried in an oven at 393 K for 2 h to remove the absorbed water and then calcined in a muffle furnace at 823 K for 4 h in an air atmosphere. This unmodified Hβ catalyst was stored in silica gel desiccators prior to use.

To prepare modified Hβ catalysts with different Sn loadings, the dried Hβ was impregnated with a solution of dibutyltin dilaurate (as Sn precursor) dissolved in toluene. Samples with various Sn loadings, given in weight percentage based on metal, were impregnated for 24 h to ensure that organic Sn compound diffused and dispersed thoroughly on the surface of Hβ. These pretreated samples were dried in an oven for 4 h at 393 K and calcined in a muffle furnace at 873 K for 4 h.

2.2. Characterization techniques

2.2.1. X-ray diffraction (XRD)

X-ray powder diffraction patterns were recorded on Rigaku C/max-2500 diffractometer using graphite filtered Cu Kα radiation ($\lambda = 1.5405$ Å) at 40 kV and 100 mA with a scanning rate of 8° min^{-1} from $2\theta = 5^\circ$ to $2\theta = 80^\circ$. The XRD phases present in the samples were identified with the help of ASTM Powder Data Files.

2.2.2. X-ray photoelectron spectroscopy (XPS)

The surface composition and the structure of catalyst were studied by X-ray photoelectron spectroscopy (XPS) in a Perkin-Elmer PHI 1600 ESCA system with Mg Kα 1253.6 eV radiation as the excitation source. The samples were mounted on the specimen holder by means of double-sided adhesive tape. Spectra were recorded in steps of 0.15 eV. The C 1s peak (284.5 eV) was used as the internal standard for binding-energy calibration. An estimated error of ±0.1 eV can be assumed for all the measurements. The scanning of the spectra was done at pressures less than 10^{-8} Torr and the temperature was approximately 293 K. Ratios of atomic concentration in the outer layers of the samples were expressed as the corresponding XPS area ratios by using the effective ionization cross-section of ejected electrons tabulated by Scofield and the formulas given by Seah and Dench [16].

2.2.3. IR studies of adsorbed pyridine

The IR spectroscopic measurements of adsorbed pyridine were carried out on a Bruker Vector 22 FTIR spectrometer with 4 cm^{-1} resolution and 500 to 4000 cm^{-1} scanning range. The samples were pressed into a 10 mg/cm^2 self-supporting wafers. Prior to each experiment, the catalysts were evacuated (1 Torr) at 693 K for 1.5 h. Then they were exposed to 303 K during 2 h. Following this, the material was exposed to 30 Torr of pyridine for 30 min, and finally evacuated for additional 1 h at 473 K. After adsorption, the samples were out-gassed and the spectra were recorded at room temperature. The treatments were carried out using a quartz IR cell [17].

2.2.4. Temperature programmed desorption of ammonia (NH_3-TPD)

NH_3-TPD experiments were conducted on a Auto-chem 2910 (Micromeritics, USA) instrument. About 100 mg of the oven-dried sample was taken in a U-shaped quartz sample tube and the sample was pretreated in ultra high pure Ar (50 ml/min) at 393 K for 1 h and then cooled to ambient temperature. The pulses of ammonia were supplied to the samples to saturate. Ammonia was replaced with argon and sample was heated to 873 K at a rate of 10 K min^{-1}.

2.3. Catalytic test

The reaction was conducted in a 250 ml glass flask equipped with a thermometer, a distillation apparatus, and

a stirrer under refluxing condition at atmosphere pressure. Especially, the top of distillation column was kept at 353 K by following through recycled hot water in order to remove methanol from the reaction system. By this means, the reaction equilibrium limitation in Reaction (1) was broken and the reaction was accelerated to develop towards the desired direction. The reaction mixture contained 0.1 mol DMO, 0.5 mol phenol and catalyst. After the raw materials and catalyst were placed into the batch reactor, nitrogen gas was flowed at 30 sccm to purge the air from the reaction system. After 10 min, nitrogen was stopped and the flask was heated at a rate of 8 K min^{-1}. The reaction was conducted at 453 K at an atmospheric pressure. Qualitative and quantitative analysis [18,19] of the reaction products and the distillates were carried out on a HP 5890-HP5971MSD and a HP 5890 gas chromatograph equipped with a flame ionization detector (FID). An OV-101packed column was used to separate products for GC analysis. The products were mainly diphenyl oxalate, methyl phenyl oxalate, anisole, and together with trace amounts of isomer products of anisole. The conversions are reported on the basis of the limiting reagent, DMO, and defined as the ratio of the moles of converted DMO to the moles of DMO fed initially to the reactor. The selectivity to MPO and DPO was defined as the moles of MPO and DPO produced per 100 mol of consumed DMO, and the yields of MPO and DPO were obtained from multiplication of DMO conversion by the selectivity to MPO and DPO.

3. Results and discussion

3.1. Catalytic activity measurements

The transesterification of DMO with phenol was carried out at 453 K under atmospheric pressure using stannum modified Hβ. Table 1 demonstrates the variation in conversion level and selectivity to MPO and DPO with Sn loadings ranging from 0% to 8%. We reported in a previous paper [12] that unmodified Hβ was an active catalyst, giving 54.0% DMO conversion, for the transesterification of DMO with phenol. However, the selectivity to DPO was only 12.2%. As shown in Table 1, when Stannum compound was added on Hβ, the selectivity to DPO was increased up to 21.0%, indicating that Stannum compound was in favor of the disproportionation of MPO into DPO. At the same time, the conversion of DMO was improved from 54.0% to 75.3% when the amount of Sn loading was 2% based on metal. And then, the conversion of DMO decreased when Sn loading was above 2%. As a result, the yield of DPO and MPO showed a maximum at 2% Sn loading.

Table 1
The catalytic performance of Hβ catalysts with different Sn loadings[a]

Sn loading (wt.%)	Conversion[b] (%)	Selectivity(%)			Yield(%)	
		AN	MPO	DPO	MPO	DPO
0	54.0	31.0	53.6	12.2	29.0	6.6
1	72.7	21.8	55.1	21.2	40.1	15.4
2	75.3	19.8	54.4	24.0	41.0	18.1
4	71.5	21.8	54.8	21.4	39.2	15.3
8	63.6	21.0	55.4	21.5	35.2	13.7

MPO: methyl phenyl oxalate, DPO: diphenyl oxalate, AN: anisole.
[a] Reaction conditions: catalyst 1.8 g, phenol 0.5 mol, PhOH/DMO = 5.0, reaction time 2 h, reaction temperature 453 K.
[b] Based on charged DMO.

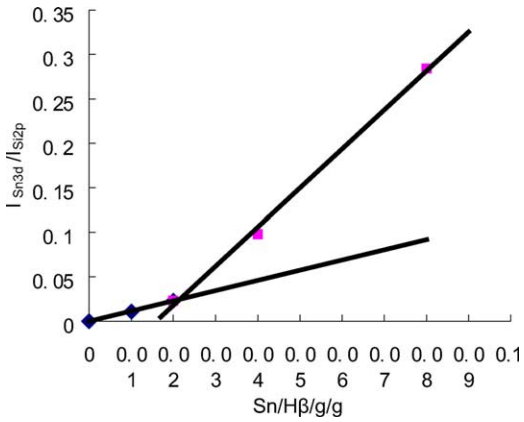

Fig. 1. Correlation between XPS peak intensity ratio of Sn 3d/Si 2p and Sn loading amount.

3.2. Quantitative analysis by XPS

XPS analysis provided bond energy values equal to 487.4 eV referring to Sn 3d, which is characteristic of Sn (IV). The Sn^{4+} peak of 487.4 eV represented SnO_2 due to dibutyltin dilaurate (DBTDL) as Sn precursor (Eq. (4)).

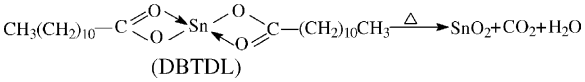

(DBTDL) (4)

It has been well established that the XPS intensity ratios of metal cations of the metal oxide to the cations of the support can provide important information regarding the dispersion and crystallite size of supported metal particles [20–23]. The relationship between the Sn 3d/Si 2p ratio and Sn content of the Sn modified Hβ samples is shown in Fig. 1. As shown in Fig. 2, there were two straight lines with different slopes corresponding, respectively to samples with Sn loading lower and higher than its dispersion capacity, and from the intercept of the two lines we can estimate the dispersed capacity of Sn on Hβ to be 2.1% Sn loading amount.

3.3. XRD analysis

The X-ray powder diffraction analysis was undertaken to determine the composition and crystallinity of Sn species. In the XRD patterns of Hβ catalysts with or without Sn modified (Fig. 2), the diffraction peaks attributed to the Hβ were

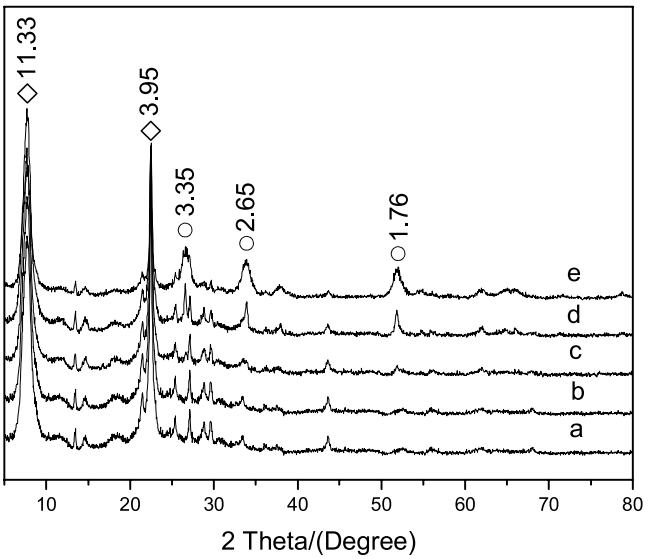

Fig. 2. XRD spectra of Hβ catalysts with different Sn loadings. (a) Hβ, (b) 1%Sn/Hβ, (c) 2%Sn/Hβ, (d) 4%Sn/Hβ, (e) 8%Sn/Hβ; (◇) Hβ, (○) SnO_2.

observed on the samples. The XRD analysis showed that there were not characteristic diffraction peaks of Sn species ($d = 0.334$, 0.264, 0.176 nm) when the loading amount of Sn was less than 4%. Whereas, when Sn loading was increased across a borderline, i.e. above its dispersion capacity, the marked change in intensity or offset of peak position can be detected at higher loadings, which indicated that Sn (IV) species was highly dispersed in the form of a monolayer at low Sn loading and SnO_2 with the tetragonal crystal structure appeared at higher loading. The appearance of SnO_2 phase led to the decrease of catalytic activity of Hβ. This result was in good agreement with the value obtained from XPS quantitative analysis.

3.4. Temperature programmed desorption of ammonia (NH_3-TPD) analysis

NH_3-TPD characterization was conducted to survey the acid strength of Hβ catalysts and the influence of Sn loading on it. In the NH_3-TPD curves, peaks are generally distributed into two regions: below and above 673 K referred to as low-temperature (LT) and high-temperature (HT) region, respectively. The peaks in the HT region can be attributed to the desorption of NH_3 from strong Brönsted and Lewis type acid sites, and the assignment of the peaks in the LT region is contributed to the desorption of NH_3 from weak acid sites [24,25]. From the results shown in Fig. 3, it can be seen that the peaks appeared both in the low and high temperature region, confirming that there existed both weak and strong acid sites on the surface of Hβ catalysts with Sn loading ranging from 0% to 8%. However, the temperature in LT region decreased about 30 K and the temperature in HT region did not vary when SnO_2 was added on Hβ. This indicated that the amount of Sn loading had effect only on

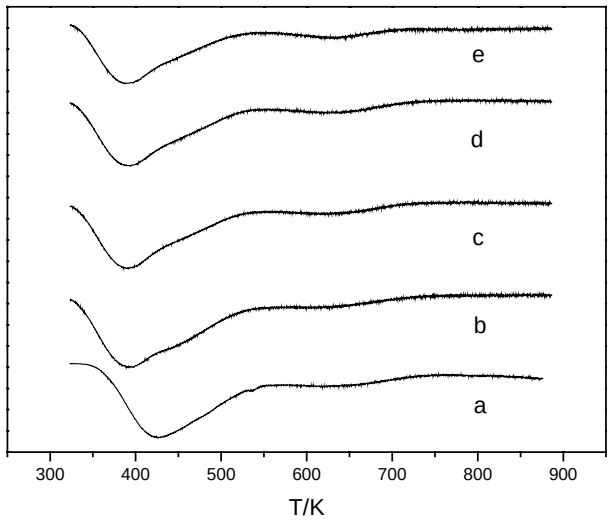

Fig. 3. NH_3-TPD profile of Hβ catalysts with different Sn loadings. (a) Hβ, (b) 1%Sn/Hβ, (c) 2%Sn/Hβ, (d) 4%Sn/Hβ, (e) 8%Sn/Hβ.

the strength of the weak surface acid sites on Hβ. We carried out a preliminary study on the effect of acid strength on the selectivity to anisole and a part of the results was reported elsewhere [12]. Briefly, the weak acid sites were responsible for the formation of MPO, while the strong acid sites were in favor of the formation of anisole. Therefore, the decrease of selectivity to anisole was not due to the change of the weak acid sites. Maybe, SnO_2 accelerated to the formation of MPO and DPO.

3.5. IR characterization of adsorbed pyridine

FTIR analysis of adsorbed pyridine allows a clear distinction between Brönsted and Lewis acid sites. IR band at 1455 cm^{-1} is attributed to pyridine adsorbed on Lewis acid

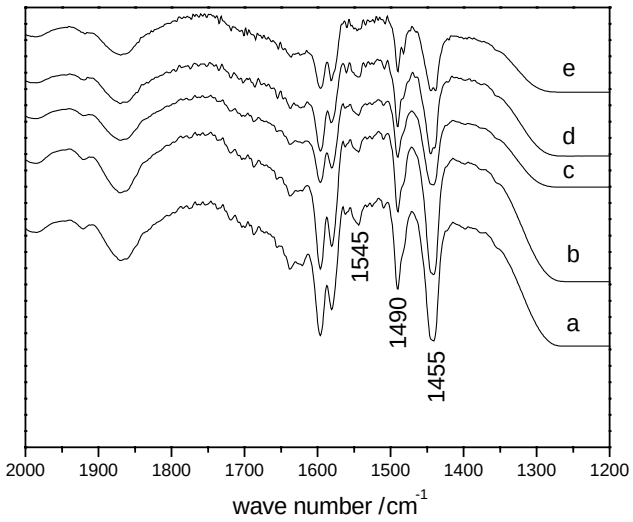

Fig. 4. FTIR spectra absorbed pyridine of Hβ catalysts with different Sn loadings. (a) Hβ, (b) 1%Sn/Hβ, (c) 2%Sn/Hβ, (d) 4%Sn/Hβ, (e) 8%Sn/Hβ.

sites, IR band at 1545 cm^{-1} to that adsorbed on Brönsted acid sites. While the peak at 1490 cm^{-1} can be ascribed to the overlapping of Brönsted acid and Lewis acid sites [26–28]. From Fig. 4, it can be seen that there were significant peaks at 1442, 1489 cm^{-1} and small peak at 1543 cm^{-1}. These indicated that many Lewis acid sites and few Brönsted acid sites were present on Hβ catalysts with or without Sn modified. The acid sites together with SnO_2 active centers catalyzed the transesterification of DMO with phenol.

4. Summary

The catalyst of Hβ with 2 wt.% Sn loading based on metal performed best, giving 75.3% conversion of DMO and 24.0% selectivity to DPO. At Sn loadings below 2 wt.%, Sn was highly dispersed as monolayer, but at higher loadings it was crystallized into bulk tin dioxide, and the catalytic activity decreased. The curve of XPS peak intensity ratio of Sn 3d/Si 2p versus Sn loading estimated the dispersed capacity of SnO_2 on Hβ to be 2.1% Sn loading amount, which was in good agreement with the value obtained from XRD analysis. NH_3-TPD results showed that the amount of Sn loading had effect only on the strength of the weak surface acid sites on Hβ. And the decrease of selectivity to anisole was not due to the change of the weak acid sites. Maybe, SnO_2 accelerated to the formation of MPO and DPO. FTIR analysis of adsorbed pyridine showed that many Lewis acid sites and few Brönsted acid sites were present on Hβ catalysts with or without Sn modified. The acid sites together with SnO_2 active centers catalyzed the transesterification of dimethyl oxalate with phenol. Especially, SnO_2 active centers were in favor of the disproportionation of MPO into DPO.

Acknowledgements

We acknowledge National Natural Science Foundation of China (no. 20276050), Tianjin Science and Technology Committee (TSTC) of China (no. 033103511) for financial support.

References

[1] A.G. Shaikh, S. Sivaram, Chem. Rev. 96 (1996) 951.
[2] Y. Ono, Pure Appl. Chem. 68 (1996) 367.
[3] K.J.L. Linsen, J. Libens, P.A. Jacobs, Chem. Commun. (2002) 2728.
[4] W.B. Kim, J.S. Lee, J. Catal. 185 (1999) 307.
[5] J.L. Gong, X.B. Ma, S.P. Wang, J. Mol. Catal. A: Chem. 207 (2004) 213.
[6] K. Okuyama, J. Sugiyama, R. Nagahata, M. Asai, M. Ueda, K. Takeuchi, J. Mol. Catal. A: Chem. 203 (2003) 21.
[7] H. Ishii, M. Goyal, M. Ueda, K. Takeuchi, M. Asai, Appl. Catal. A: Gen. 201 (2000) 101.
[8] K. Nishihira, S. Tanaka, K. Harada, R. Sugise, US Patent 5 834 615 (1997).
[9] K. Nishihira, S. Tanaka, K. Harada, R. Sugise, A. Shiotani, K. Washio, US Patent 5 922 827 (1999).
[10] T. Matsuzaki, A. Nakamura, Catal. Surv. Jpn. 1 (1997) 77.
[11] K. Nishihira, S. Tanaka, Y. Nishida, I. Hirofumi, S. Fujitsu, K. Harada, US Patent 5 811 573 (1998).
[12] S.P. Wang X.B. Ma, H.L. Guo, in: Proceedings of the Fifth International Symposium on Green Chemistry, China, May 22–26, 2002.
[13] I. Gabriello, R. Ugo, T. Renato, Ger. Offen. 2 528 412 (1976).
[14] T. Hideaki, O. Yoshiyuki, M. Atusi, EP 684 221 (1995).
[15] I. Masashi, S. Kohei, T. Tatsuro, JP 08 188 588 (1996).
[16] M.P. Seah, W.A. Dench, Surf. Interface Anal. 1 (1979) 2.
[17] J. Foschiera, T. Pizzolato, E. Benvenutti, J. Brazil Chem. Soc. 12 (2001) 159.
[18] S.P. Wang, Z.H. Li, X.B. Ma, G.H. Xu, Chinese J. Anal. Chem. 30 (7) (2002) 829.
[19] S.P. Wang, X.B. Ma, Z.H. Li, G.H. Xu, Chinese J. Anal. Chem. 30 (9) (2002) 1085.
[20] Y.C. Xie, Y.Q. Tang, Adv. Catal. 37 (1990) 1.
[21] L. Salvati Jr., L.E. Makovsky, J.M. Stencei, F.R. Brown, D.M. Hercules, J. Phys. Chem. 85 (1981) 3700.
[22] S.C. Fung, J. Catal. 58 (1979) 454.
[23] L. Dong, Y. Chen, J. Chem. Soc., Faraday Trans. 92 (1996) 4589.
[24] F. Lónyi, J. Valyon, Micropor. Mesopor. Mat. 47 (2001) 293.
[25] M. Sawa, M. Niwa, Y. Murakami, Zeolites 10 (1990) 532.
[26] T. Barzetti, E. Selli, D. Moscotti, L. Forni, J. Chem. Soc., Faraday Trans. 92 (1996) 1401.
[27] T.R. Hughes, H.M. White, J. Phys. Chem. 71 (1967) 2192.
[28] C.A. Emeis, J. Catal. 141 (1993) 347.